




ARTICLE

DOI: 10.1038/s41467-018-04584-z

OPEN

Artificial strain of human prions created in vitro

Chae Kim¹, Xiangzhu Xiao², Shugui Chen^{2,4}, Tracy Haldiman¹, Vitautas Smirnovas^{2,5}, Diane Kofskey¹, Miriam Warren¹, Krystyna Surewicz², Nicholas R. Maurer ¹, Qingzhong Kong ^{1,3}, Witold Surewicz ^{1,2} & Jiri G. Safar^{1,3}

The molecular mechanism that determines under physiological conditions transmissibility of the most common human prion disease, sporadic Creutzfeldt-Jakob disease (sCJD) is unknown. We report the synthesis of new human prion from the recombinant human prion protein expressed in bacteria in reaction seeded with sCJD MM1 prions and cofactor, ganglioside GM1. These synthetic human prions were infectious to transgenic mice expressing non-glycosylated human prion protein, causing neurologic dysfunction after 459 and 224 days in the first and second passage, respectively. The neuropathology, replication potency, and biophysical profiling suggest that a novel, particularly neurotoxic human prion strain was created. Distinct biological and structural characteristics of our synthetic human prions suggest that subtle changes in the structural organization of critical domains, some linked to posttranslational modifications of the pathogenic prion protein (PrP^{Sc}), play a crucial role as a determinant of human prion infectivity, host range, and targetting of specific brain structures in mice models.

¹Department of Pathology, Case Western Reserve University, 2085 Adelbert Rd, Cleveland, OH 44106, USA. ²Departments of Physiology and Biophysics, Case Western Reserve University, 2085 Adelbert Rd, Cleveland, OH 44106, USA. ³Department of Neurology, Case Western Reserve University, 2085 Adelbert Rd, Cleveland, OH 44106, USA. ⁴Present address: GlaxoSmithKline, 709 Swedeland Rd., King of Prussia PA19406, UK. ⁵Present address: Department of Biothermodynamics and Drug Design, Institute of Biotechnology, Vilnius University, Graiciuno 8, Vilnius 02241, Lithuania. Correspondence and requests for materials should be addressed to J.G.S. (email: jiri.safar@case.edu)

Human prions cause invariably fatal, rapidly progressive neurodegenerative diseases, formerly called transmissible spongiform encephalopathies (TSEs)^{1,2}. Approximately 90% of human prion diseases are sporadic, 10% are associated with pathogenic mutations in PRNP gene, and 1% is caused by zoonotic or iatrogenic prion infection. Despite relatively low frequency of transmitted human prion diseases, they have gained considerable importance due to their long incubation time and high resistance of human prions to inactivation, posing unprecedented and challenging problems to disease control and public health³. These invariably fatal neurodegenerations are caused by a pathogenic protein, PrP^{Sc}, which is a misfolded isoform of the normal cellular prion protein^{5–11}, PrP^C. Human prions exist as a broad spectrum of strains corresponding to at least eight diverse clinicopathological disease phenotypes; may undergo mutation and further evolution¹². High-resolution structure of human prions and the mechanism of their formation as well as remarkably precise anatomical targeting to different brain structures remain unknown. Many basic concepts in prion research (including that of prion strains) as well as the current strategies for therapeutic interventions were based on studies with laboratory rodent prions. Even though these studies have provided fundamentally important insights, the lessons from these studies do not apply directly to human prion diseases, as evidenced, for example, by several recently failed clinical trials^{13–15}. One of the key reasons behind these disappointing results are fundamental differences between human prions causing diseases such as sporadic Creutzfeldt-Jakob disease (sCJD) and cloned laboratory prions¹⁶. In particular, our recent experiments indicate that replication of sCJD prions is principally determined by growth rate of prion aggregates that is in turn controlled by their specific structural features, and not by their conformational stability, as it is in yeast and some murine prions¹⁶. How these aspects impact transmissibility of prions to man is an imperative question in light of history of iatrogenic and zoonotic transmissions and recent findings of human prions in the skin and body fluids^{17,18}.

A number of recent studies have demonstrated that infectious rodent prions can be generated in vitro from bacterially expressed recombinant mouse or Syrian hamster PrP^{19–23}, and the infectivity titer of some of these preparations was very high^{19,21}. These studies played a fundamentally important role in providing the ultimate proof for the protein-only hypothesis of prion diseases^{21,22,24–27}. However, attempts to generate infectious synthetic human prions have not yet been successful, hindering efforts to comprehensive understanding of human prion diseases such as sCJD. Here we bridge this gap, showing that human prions can be synthesized in vitro from bacterially expressed recombinant human PrP in a reaction seeded with sCJD MM1 prions in the presence of a novel cofactor, ganglioside GM1. These synthetic human prions appear to have unique strain properties. By comparing the structural organization of these synthetic human prions with that of parent sCJD MM1 prions and noninfectious human prion protein amyloid, we have identified domains in PrP that are important for the initiation of replication in vivo, i.e. their infectivity, and for targeting of different anatomical brain structures. These structural and functional insights provide a foundation for more complete understanding of the molecular basis of human prion formation and propagation.

Results

Generation of recombinant human prions. Using our 96-well plate-formatted quaking-induced conversion (QuIC) and the recombinant human full-length prion protein [huPrP

(23–231,129 M)] substrate^{16,28,29}, we first systematically screened a broad range of experimental conditions (temperature, time, recHuPrP concentration, different cofactors) for the seeded and unseeded conformational conversion reactions (Supplementary Tables 1, 2, 3, and 4). The use of conformation-dependent immunoassay (CDI) and conformational stability assay (CSA) gave us an opportunity to monitor not only the amount of the conversion product, but also to screen the conformational fidelity of the conversion reactions by comparing the conformational stability of each reaction product with that of the seed. The selection criteria for the conversion products to be used in the subsequent bioassay experiments were as follows: minimized spontaneous conversion in the absence of the seed, high yield of the conversion reaction, and similarity of conformational stability of the product and the seed. As shown in Supplementary Table 3 and Supplementary Fig. 1, in the presence of sCJD MM1 seed the reaction performed at 37 °C in a PBS (pH 6.9) containing 0.1% (w/w) Triton X100, 0.7 mM monosialoganglioside (GM1), and 0.02 mM polyadenylic acid (PolyA) was characterized both by high amplification rate as well as the final product showing conformational stability essentially identical to that of the original sCJD MM1 prion seed. Interestingly, the most efficient cofactor for amplification of sCJD MM2 prions to conformationally similar replicas was not GM1 but another lipid, 1-palmitoyl-2-oleoyl-sn-glycero-3-phospho(1'-rac-glycerol) (Supplementary Fig. 1a and Supplementary Fig. 1b, Supplementary Tables 1, 2, 3, and 4).

Based on these data, and given that sCJD MM1 prions are known to replicate in transgenic mice much more efficiently than the MM2 counterparts^{30–32}, we selected for further studies recombinant PrP replicas generated in the reaction seeded with sCJD MM1 prions in the presence of GM1. Importantly, no spontaneous (i.e., non-seeded) zconversion of recHuPrP was observed under the same experimental conditions (Supplementary Fig. 1a). First, we analyzed these replicas by far-UV circular dichroism spectroscopy (Fig. 1a), finding that they are characterized by high content of β -sheet structure (~41% vs. 3% for PrP monomer in the native conformation). Since the starting brain concentrations and purification yields of sCJD PrP^{Sc} are very low (~200-fold lower compared to rodent PrP^{Sc}), no high quality CD spectrum could be obtained for the seed. Nevertheless, the content of β -structure in the recombinant PrP sCJD replicas is similar to that previously reported for rodent prions⁵.

To further examine the degree of structural fidelity of the replication of sCJD MM1 prions using the recombinant PrP substrate and our present experimental conditions, we used two mass spectrometry-based methods: histidine hydrogen/deuterium exchange mass spectrometry (His-HXMS) and backbone amide hydrogen/deuterium exchange coupled with mass spectrometry (HXMS). These methods have been shown to be uniquely well suited for structural analysis of not only recombinant PrP aggregates but also brain-derived PrP^{Sc}^{16,33–36}.

His-HXMS monitors water accessibility of individual His side chains³⁷, providing residue-specific information about the packing and interfaces between β -sheets in ordered protein aggregates^{16,33,36}. As shown in Fig. 1b, four out of five His residues in the PK-resistant region are characterized by distinct environments in brain-derived sCJD MM1 PrP^{Sc} and its recombinant PrP replica, as indicated by substantial differences in the rate of H/D exchange for C2 protons in histidine imidazole rings. This clearly indicates distinct packing arrangements within the two types of PrP aggregates examined. Structural differences between sCJD MM1 PrP^{Sc} seeds and recombinant PrP products of the conversion reaction are further indicated by HXMS studies that probe the rate of H/D exchange of the backbone amide hydrogens^{33–36,38}. These structural differences are particularly

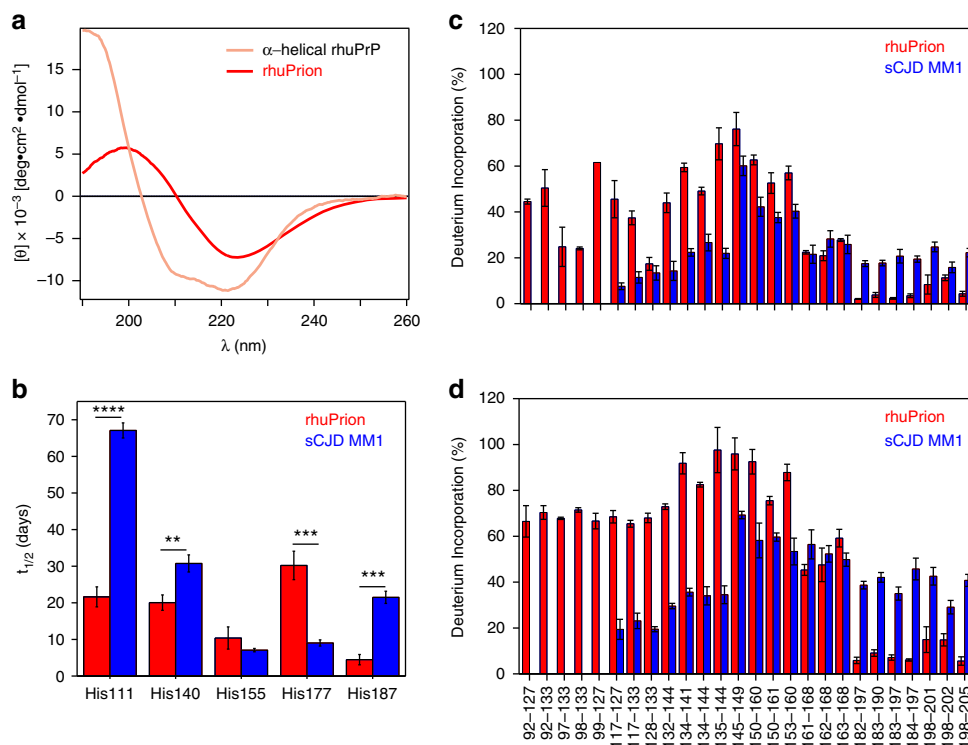


Fig. 1 Structural comparison of rhuPrion and brain-derived sCJD MM1 PrP^{Sc} used as an initial seed. **a** Far UV circular dichroism (CD) spectrum of recombinant human PrP monomer used as a QuIC substrate, and rhuPrion. **b** Histidine H/D exchange (His-HXMS) for rhuPrion (red) and MM1 rPrP^{Sc} (blue). The parameter $t_{1/2}$ represents the half-time of exchange reaction for individual His residues. Error bars indicate standard deviation (3 independent experiments). ** $p < 0.01$; *** $p < 0.001$. **c, d** Backbone amide H/D exchange (HXMS) data for peptic fragments derived from rhuPrion (red) after 5 min (**c**) and 24 h (**d**) incubation in D₂O. For comparison, previously published data are included for sCJD MM1 rPrP^{Sc} (blue) data after 5 min (**c**) and 10 days (**d**) incubation in D₂O¹⁶. Error bars indicate standard deviation (3 independent experiments). * $p < 0.05$; ** $p < 0.02$

pronounced in the region between residues ~117 and 144. Peptic fragments from this region in the recombinant PrP product show substantially higher degree of H/D exchange compared to that in the sCJD MM1 seed already after 5 min of incubation in D₂O (Fig. 1c), and these differences become even more dramatic after longer incubation times. Indeed, in the recombinant PrP product this region shows more than 65% exchange after 24 h, whereas in brain PrP^{Sc} it remains highly protected even after 10 days of incubation in D₂O (Fig. 1d). By contrast, the region between residues ~182 and 205 appears to be less prone to deuterium labeling (and thus more ordered) in the recombinant PrP product than in the brain-derived sCJD MM1 seed. Altogether, these data demonstrate that, in the presence of GM1 as a cofactor, sCJD MM1 prions can efficiently seed the conversion of the recombinant PrP to β -sheet-rich aggregates. However, the structure of this product is not identical to that of the seed. One of the factors contributing to apparently imperfect conformational fidelity of this seeded conversion reaction could be the lack of post-translational modifications (GPI anchor, glycosylation of Asn residues) in the recombinant PrP substrate used.

Bioassays of recombinant replicas of human prions. To test the infectivity of the recombinant PrP replicas of sCJD MM1 prions, we performed ten rounds of QuIC (all in the presence of polyA and GM1), initially seeded with 0.1% brain homogenate of sCJD MM1 human brain. The initial reaction concentration of seed PrP^{Sc} was 0.126 ng/ml and recombinant PrP 0.1 mg/ml, corresponding to the seed/substrate mass ratio ~1:1,000,000. Each subsequent nine rounds were seeded with 10-fold diluted product

from the previous round, resulting in a cumulative 10^{-13} dilution of the original brain prions and PrP^{Sc} seed to 0.1 ag of PrP^{Sc}, an amount ~100,000 times below one infectious dose unit of sCJD prions³⁹ (Fig. 2a). Even though the conditions were the same in all cycles, the conformational stability of the reaction products shifted gradually in each cycle, with Gdn HCl concentration corresponding to the midpoint denaturation moving from 3.06 M for the original sCJD MM1 PrP^{Sc} to 2.56 M for the reaction product after 10 rounds of QuIC (Fig. 2a). Furthermore, less cooperative conformational transition was observed with an increase in the number of QuIC rounds. We interpret these observations as indicative of a broadening of the spectrum of conformers with lower average stability than that of the original seed.

We inoculated with the amplified material transgenic mice Tg40 that express human PrP(129 M) with native protranslational modifications (i.e., glycosylation of Asn residues and the GPI anchor)⁴⁰ as well as transgenic mice TgNN6h that express human PrP(129 M) in which glycosylation was abolished by N181Q and N197Q substitutions¹². The latter line of transgenic mice was selected for high levels of cell surface expression of unglycosylated PrP^C after monitoring white blood cells by FACS in founder's mice. Even though it is known that glycosylation per se has no effect on the 3D structure of PrP⁴¹, we further verified that the N181Q and N197Q substitutions do not affect the overall folding of the protein. Indeed, recombinant wild-type and mutant proteins show indistinguishable far-UV CD spectra and are characterized by essentially identical thermodynamic stability (Supplementary Fig. 2). It was also verified that the N181Q/N197Q PrP^C in TgNN6h mice is cell-surface expressed and contains the GPI anchor (as indicated by immunochemical

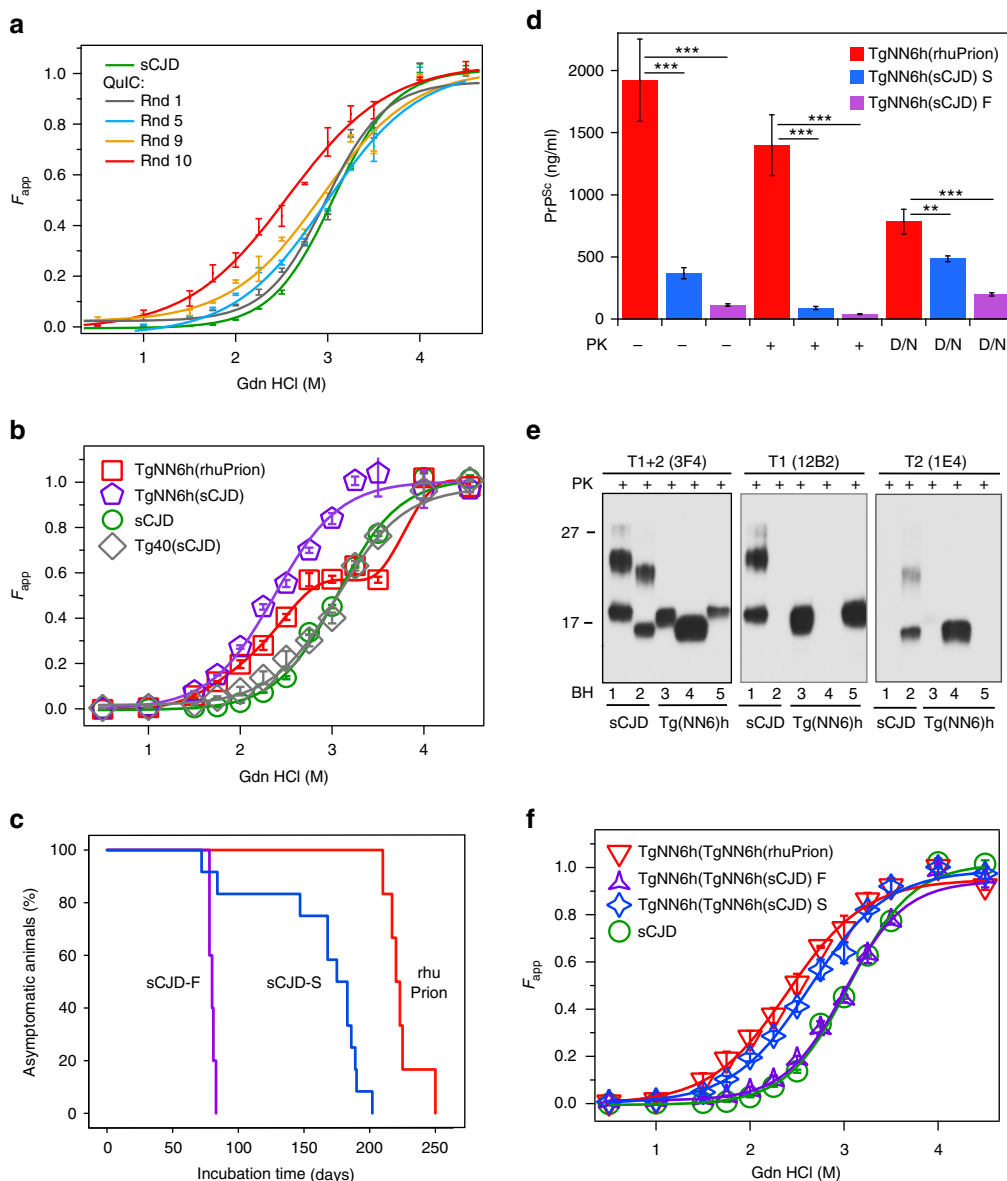


Fig. 2 Biochemical properties of rhuPrion. **a** Conformational stability of serial QuIC products. The reaction in the first round (Rnd1) was seeded with brain-derived sCJD MM1 prions. **b** Conformational stability profiles of rhuPrion and sCJD prions after the first passage in TgNN6h or Tg40 mice. **c** Survival curves of rhuPrion, sCJD-S, and sCJD-F prions in the second passage in TgNN6h. **d** Levels of total PrP^{Sc}, protease-resistant PrP^{Sc}, and D/N ratio using CDI assay of brain homogenates upon the second passage of different prions in TgNN6h mice. **e** Western blots of prion isolates probed with antibodies detecting both Type 1 and Type 2 PrP^{Sc} (3F4) and antibodies specific for Type 1 (12B2) or Type 2 (1E4) PrP^{Sc}: lane 1—MM1 sCJD; lane 2—MM2 sCJD; lane 3—rhuPrion; lane 4—sCJD-F prions; lane 5—sCJD-S prions. **f** Conformational stability profiles of the original human brain-derived sCJD, rhuPrion, and sCJD prions after the second passage in TgNN6h mice

examination of brain tissue and the release of PrP^C into Tx114 aqueous phase upon PIPLC treatment (Supplementary Fig. 3)⁴². While no disease was observed in Tg40 mice inoculated with the recombinant PrP replica of sCJD MM1 prions, clinical symptoms of prion disease were observed in 60% of TgNN6h mice inoculated with the same preparation, with an average incubation time of 459 days (Table 1). In control experiments it was verified that brain-derived sCJD MM1 prions (used as a seed in our conversion reaction *in vitro*) triggered disease in both TgNN6h and Tg40 lines, with incubation times of ~417 days and ~169 days, respectively. Neither β -sheet-rich aggregates generated without seeds according to the previously published protocol³⁵, nor native monomers of reHuPrP induced clinical symptoms, and the neuropathology of aged-matched Tg40 and TgNN6h mice showed no abnormalities or deposition of pathogenic prion

protein (Table 1). The conformational stability of PrP^{Sc} accumulating in Tg40 mice inoculated with sCJD MM1 prions matched the stability of the PrP^{Sc} in the inoculum. By contrast, the stability of PrP^{Sc} accumulating in the brains of TgNN6h mice inoculated with the same inoculum was significantly reduced, as indicated by lower value of [Gdn HCl]_{1/2} (Fig. 2b). TgNN6h mice inoculated with the recombinant replica of MM1 sCJD prions accumulated PrP^{Sc} characterized by biphasic denaturation curves, with ~60% of conformers having stability similar to that of PrP^{Sc} in sCJD-infected mice and ~40% having higher stability (Fig. 2b). Importantly, all TgNN6h mice inoculated with brain homogenate from the first passage of recombinant PrP prion replicas (rhuPrion) developed clinical symptoms, with the average incubation time of 224 days (Table 1; Fig. 2c). A particularly intriguing phenomenon was observed in the second passage of

Table 1 Serial transmission experiments in transgenic mice expressing glycosylated and unglycosylated human PrP(129 M)

Inoculum	Host	PrP expression level n-fold	Mean IT Days ± SEM	Prion positive n/n ₀	PrP ^{Sc} [Gdn HCl] _{1/2} M ± SEM
Primary host and transmission					
sCJD MM1	Human	–	–	–	3.06 ± 0.03
rHuPrion	Tg(HuPrP ^{N181,197Q} ,129 M)	0.6	459 ± 114	6/10	2.65 ± 0.18
	Tg(HuPrP, 129 M)	1	>700	0/10	–
sCJD MM1	Tg(HuPrP ^{N181,197Q} ,129 M)	0.6	417 ± 32	3/3	2.38 ± 0.04
	Tg(HuPrP, 129 M)	1	169 ± 12	10/10	3.07 ± 0.05
HuPrP(α-monomer)	Tg(HuPrP ^{N181,197Q} ,129 M)	0.6	>716	0/9	–
	Tg(HuPrP, 129 M)	1	>700	0/10	–
huPrP(β-aggregates)	Tg(HuPrP ^{N181,197Q} ,129 M)	0.6	>716	0/6	–
	Tg(HuPrP, 129 M)	1	>700	0/10	–
Secondary transmission					
rhuPrion	Tg(HuPrP ^{N181,197Q} ,129 M)	0.6	224 ± 6	6/6	2.40 ± 0.05
sCJD MM1-F	Tg(HuPrP ^{N181,197Q} ,129 M)	0.6	80 ± 1	5/5	3.01 ± 0.04
sCJD MM1-S	Tg(HuPrP ^{N181,197Q} ,129 M)	0.6	162 ± 12	12/12	2.64 ± 0.04

PrP expression levels were determined relative to the expression of mouse PrP in FVB mice
n number of prion positive mice, n₀ number of mice under observation

sCJD MM1 prions in TgNN6h mice, as these mice clearly segregated into two distinct groups: one with the average incubation time of 162 days (denoted sCJD-S, where S stands for slow) and the second one with the average incubation time of 80 days (denoted sCJD-F, where F stands for fast) (Table 1; Fig. 2c). Cumulatively, these experiments indicate that: glycosylation of the host PrP^C is important for conformational fidelity of sCJD prions replication *in vivo*, unglycosylated host PrP^C provides an efficient substrate for the replication of synthetic human prions (rhuPrions) generated from an unglycosylated recombinant prion protein, and sCJD prions can propagate in mice expressing unglycosylated PrP^C as two distinct strains, one of which is characterized by a remarkably short incubation time. Such subcloning of a single human prion isolate into two or more distinct strains has been described previously in transgenic mice^{30,32} as well as in cell cultures⁴³ and led to the notion that wild prion isolates actually consist of a mixture (“cloud”) of diverse molecular assemblies¹⁰. Whether this strain heterogeneity observed in the present study is at least partly related to the Asn to Gln substitutions positions 181 and 197 necessary to eliminate the two N-linked glycosylation sites on human PrP is not known. However, these amino acid substitutions are generally considered as highly conservative, and circular dichroism (CD) spectroscopy data indicate no conformational impact on PrP^C (Supplementary Fig. 2).

In the second passage of rhuPrions in TgNN6h mice, these mice accumulated ~5 and 15-fold more PrP^{Sc} than mice infected with sCJD-F and sCJD-S strains, respectively, and the same trends were observed for proteinase-resistant PrP^{Sc} (rPrP^{Sc}) (Fig. 2d). Different denatured/native (D/N) ratios of PrP^{Sc} antibody epitopes (3F4 epitopes 108–112 and 8H4 epitope 175–185) indicate that they are variably exposed in the native state of mice inoculated with different inocula, confirming distinct conformations as detected by CSA (Fig. 2d). Furthermore, Western blot typing with a set of differentiating antibodies revealed that TgNN6h mice inoculated with rhuPrions accumulated Type 1 rPrP^{Sc}, whereas those inoculated with sCJD-S and sCJD-F prions accumulate Type 1 and Type 2 rPrP^{Sc}, respectively (Fig. 2e). While PrP^{Sc} from sCJD-F strain shows CSA profiles superimposable with those for the original human brain-derived sCJD MM1 PrP^{Sc}, the nearly superimposable CSA profiles of PrP^{Sc} in rhuPrions and sCJD-S prions shifted to the lower stability (Table 1; Fig. 2f). We conclude from these observations that inoculation with rhuPrions leads to the accumulation of very

high levels of PrP^{Sc} with distinct Type 1 conformational characteristics and stability, whereas the original sCJD MM1 prions cloned in TgNN6h into two isolates, one with short incubation time and Type 2 rPrP^{Sc} conformers and the other one with long incubation time and Type 1 rPrP^{Sc}.

Comparative neuropathology of rhuPrion. Three distinct vacuolization profiles for TgNN6h mice inoculated with rhuPrion and original MM1 sCJD prions were identified. The rhuPrion pattern exceeded the vacuolization profiles of both subclones of MM1 sCJD prions, most prominently in the cortex, hippocampus, subiculum, basal ganglia, and hypothalamus. These distinct lesion profiles found in rhuPrion-inoculated TgNN6h mice were preserved upon second passage (Fig. 3a, b, c), indicating that rhuPrion represents a stable strain that is distinct from two subclones of the original sCJD MM1 prions. Remarkably, both in the first and second passage, CA3 pyramidal layer cells of hippocampus were completely destroyed and replaced by confluent vacuoles. Some of the vacuoles were proximal to large deposits of PrP^{Sc} and appeared reminiscent of florid plaques found in vCJD cases. The same hippocampal structures were either intact in sCJD-S subclone or all hippocampal formation structures were affected indiscriminately in sCJD-F subclone (Fig. 3a, b). Moreover, the first and second passage of rhuPrion led to widespread thioflavin S positive plaques of PrP^{Sc}, most prominently in the hippocampus and cortex (Fig. 3c, d). In contrast, sCJD-F clone was characterized by fine, evenly distributed deposits of PrP^{Sc} with synaptic-like pattern, and the infection with sCJD-S prion clone resulted in small preamyloid deposits of PrP^{Sc} in the hippocampus and in the cortex. These data indicate that rhuPrions represent a distinct human prion strain that, apart from cortex and other gray matter, specifically targets cells in the CA3 pyramidal layer of hippocampus and leads to the accumulation of high levels of PrP^{Sc} forming amyloid plaques in the hippocampus and cortex.

Second passage rhuPrions from TgNN6h mice brains could be replicated *in vitro* by protein misfolding cyclic amplification using Tg40 mice brain homogenate as a substrate. The replication rate was paradoxically lower for sCJD-F subclone, and both rhuPrion and sCJD-S replicated with comparable rates (Fig. 4a). These results indicate that unglycosylated prions present in TgNN6h isolates, including rhuPrions, can be replicated using fully posttranslationally processed normal human PrP^C substrate. The end-point titration of seeding activity of all three TgNN6h

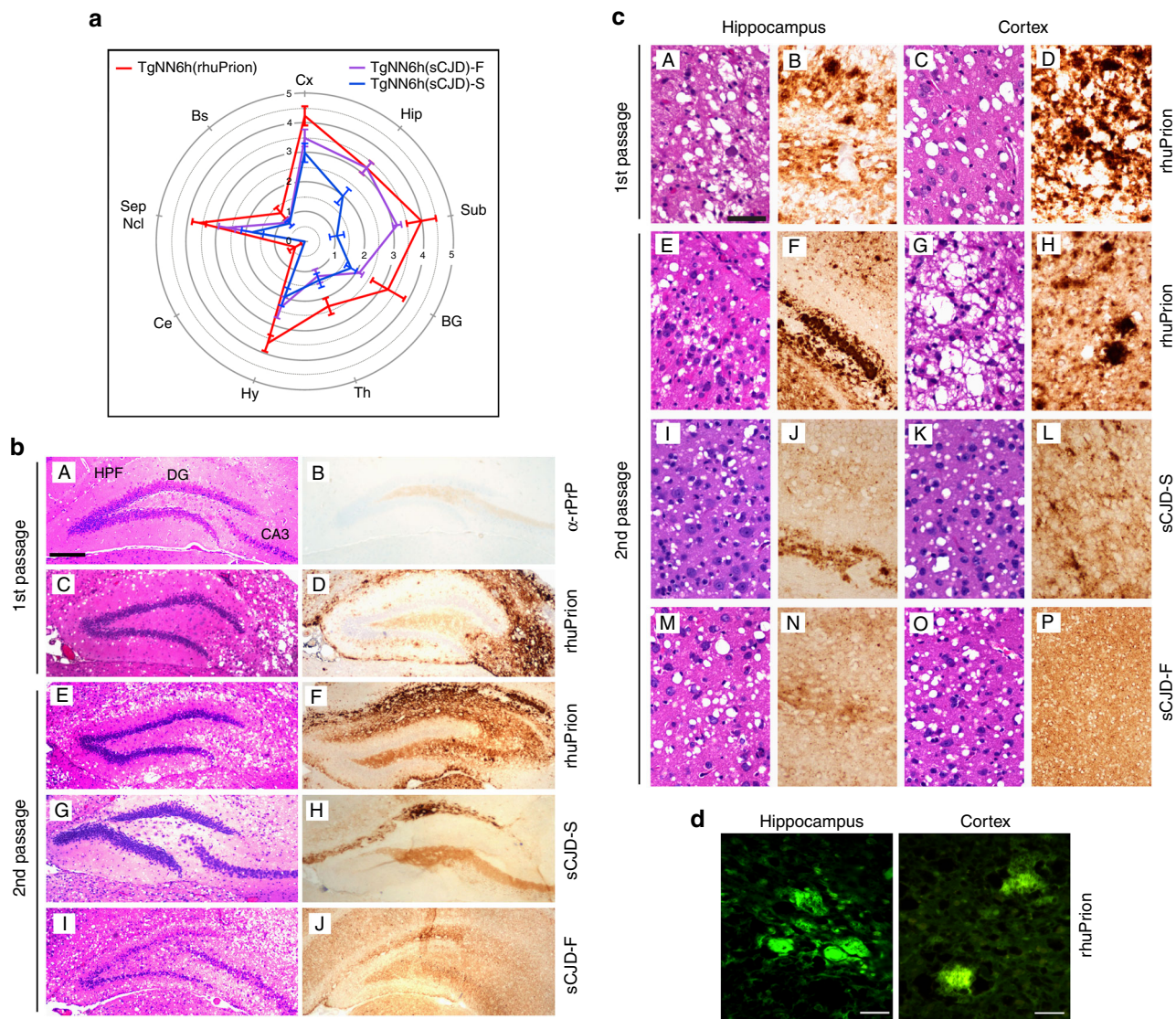


Fig. 3 Neuropathological profiles of rhuPrion and sCJD prions in TgNN6h mice. **a** Semi quantitative vacuolization scoring within the indicated brain regions of rhuPrion and sCJD prions in TgNN6h mice: Cx, cortex; Hip, hippocampus; Sub, subiculum; BG, basal ganglia; Th, thalamus; Hy, hypothalamus; Ce, cerebellum; Sep Ncl, septal nuclei; Bs, brain stem. **b** Neuropathology panels of hippocampus formation (HPF) of age-matched TgNN6h mice inoculated with alpha-helical monomers of human prion protein (**A, B**), rhuPrion (**C, D**) in the first and (**E, F**) second passage; panels **G, H, I, J** show distinct characteristics of second passage of sCJD-S and sCJD-F prions. **c** Extensive neuronal loss and vacuolization in the CA3 pyramidal layer of hippocampus (**A**) and in the cortex (**C**) in the first (**A, C**) and second (**E, G**) passage of rhuPrion in contrast to less prominent loss in TgNN6h mice inoculated with sCJD-S (**I, K**) and sCJD-F (**M, O**) prions as visualized by H&E staining. Extensive PrP^{Sc} depositions in the stratum oriens of CA1 hippocampal formation and cortex following first (**B, D**) or second (**F, H**) passage of rhuPrions. Distinctly different patterns of depositions of PrP^{Sc} in sCJD-S and sCJD-F prions in both hippocampus (**J, N**) and cortex (**L, P**) of TgNN6h mice. **d** Thioflavin S positive amyloid plaques in the hippocampus and cortex of TgNN6h mice inoculated with rhuPrion. Vacuolization was visualized by H&E staining, and PrP^{Sc} deposition was assessed by immunohistochemistry with the antibody 3F4. HPF, Hippocampus formation; DG, granule cell layer of the dentate gyrus; CA3, pyramidal layer of hippocampus

prion isolates in RT QuIC with SHa(PrP90-231) (Fig. 4b) and with Bv(23-231) (Fig. 4c) substrates indicates that rhuPrion has a seeding titer ~100-fold and 1000-fold higher compared to sCJD-S and sCJD-F prions, respectively. Since the concentration of PrP^{Sc} in rhuPrions brain homogenates was only ~twofold higher than that of PrP^{Sc} in sCJD-S and sCJD-F homogenates (Fig. 4a), this remarkably high seeding potency suggest that rhuPrion is composed of unique conformers with exceptionally high capacity to convert PrP monomers into Thioflavin-positive β -sheet aggregates. The nonequilibrium sedimentation velocity profile of rhuPrion and both sCJD isolates were similar, with the highest concentration of PrP^{Sc} in the bottom of the tubes (Fig. 4d, e, f). Based on previous calibration²⁹, we estimate that the prevalent

population of aggregates in rhuPrions has a mass of at least 14×10^6 Da, which corresponds to at least 600 monomers of PrP^{Sc}.

Discussion

The pathogenic conformer of human prion protein—PrP^{Sc}—is an essential and possibly the only constituent of infectious human prions. However, a high-resolution structure of human PrP^{Sc} is lacking, and the molecular mechanism that determine initiation and propagation under physiological conditions—prion infectivity—remain obscure^{16,44}. Our present study demonstrates, for the first time, that infectious human prion can be generated in vitro

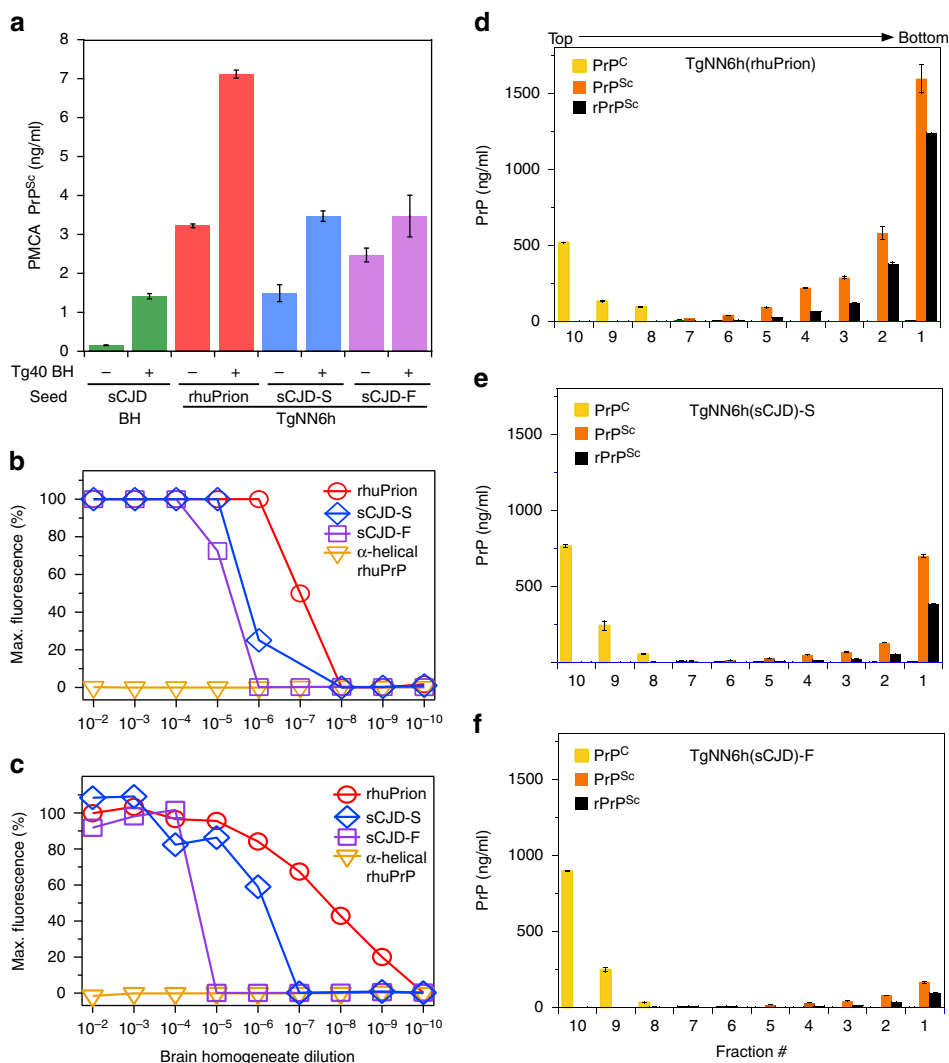


Fig. 4 Replication potency and sedimentation velocity of rhuPrion, sCJD-S, and sCJD-F prions. **a** Amplification of rhuPrion, sCJD-S, and sCJD-F prions by sPMCA using as a substrate brain homogenate of Tg40 mice expressing fully posttranslationally processed human PrP^C (129 M). The concentration of PrP^{Sc} before and after PMCA was measured with CDI. The second generation of RT QuIC (seeded with rhuPrion, sCJD-S, and sCJD-F prions) using recombinant SHa(PrP90-231) (**b**) and recombinant Bv(23-231) (**c**) as a substrate. Data points represent relative Thioflavin T fluorescence of the positive control reference and end point dilution of the seeds in four RT QuIC experiments. Sedimentation velocity profiles of rhuPrion (**d**), sCJD-S (**e**), and sCJD-F prions (**f**). The samples were fractionated by ultracentrifugation in sucrose gradient, and fractions were collected from the bottom of the tubes and analyzed for PrP^{Sc} by CDI. The bars represent average \pm SEM; CDI was performed on each sCJD sample in triplicate

from the bacterially expressed recombinant human prion protein in a reaction seeded with brain-derived sCJD prions. Furthermore, our experiments reveal that, even though many conditions are conducive to efficient propagation of PrP aggregates in vitro upon seeding with human prions, they do not always cause the development of prion disease in vivo. The infectivity and pathogenicity, as well as specific targeting of neurons in different brain structures in vivo appear to be controlled by seemingly subtle differences in the conformation, especially in the C-terminal domain that of PrP that is involved in posttranslational modifications.

Although the infectivity of the herein described new artificial prion in the first passage was relatively low and limited to the transgenic mice line expressing unglycosylated human PrP, the bioassay revealed a particularly destructive neuropathological phenotype with widespread vacuolization and loss of neurons, particularly in the CA3 (Cornu Ammonis) region of hippocampus, and numerous Thioflavin S-positive plaques. The CA3 region has attracted major attention in recent years for its specific

role in memory processes and in susceptibility to seizures, and the synthetic human prion offers a new powerful tool to study the pathophysiology of neurodegeneration in this area, especially relevant to Alzheimer’s disease. While these intriguing findings may suggest generally lower fidelity of in vitro replication of brain derived prions with unglycosylated substrate, another possibility is that posttranslational modification of prion protein—glycosylation and glycosylphosphatidylinositol (GPI) anchor—are important determinants of conformational fidelity in serial propagation in vitro and also in the transmissibility (infectivity) of prions in vivo⁴⁵. Even though some aspects of the latter possibility have recently been suggested based on experiments with cell-adapted prions and rodent prion strains^{43,46,47}, to fully understand the impact of posttranslational modifications on the structural fidelity of human prion replication to the infectious form, it will be critical to perform a structural and functional comparison of conversion reactions using recombinant PrP substrates in which one can systematically alter the type of specific modifications.

The discovery of variable glycosylation patterns and heritable polymorphic PK cleavage sites of human brain PrP^{Sc} markedly differentiated early on human prions from cloned laboratory prions of animal origin^{48–50}. The subsequent experiments with more sensitive biophysical tools revealed a wide spectrum of sCJD PrP^{Sc} structural states and interplay with distinct glycosylation patterns in each clinicopathological category of human prion diseases, and argued for a broad spectrum of human prion strains coding for different phenotypes^{29,51,52}. Moreover, our most recent data demonstrate that typical human prions causing sporadic Creutzfeldt-Jakob disease (sCJD) differ in a major way from both cloned laboratory prions and synthetic prion amyloids¹⁶. Importantly, phenotypically very distant MM1 and MM2 sCJD prions differ in their structural organization, specifically in the polypeptide backbone and quaternary structure (packing) of prion particles. These unique structural features primarily control the replication rate of human prions¹⁶. Finally, our *in vitro* data reported here suggest that this aspect is in turn controlled (probably kinetically) by strain-specific auxiliary molecules differentially facilitating conversion reactions of some prion strains but not others.

The existence of auxiliary molecules facilitating PrP^{Sc} formation and replication was first suggested from the co-purification of Syrian hamster PrP^{Sc} with sphingolipids, galactosylceramide, and sphingomyelin⁵³, and with 25-mer polynucleotides encoding variable sequences³⁹. This hypothesis was supported more recently by the findings that the PMCA conversion of purified brain-derived PrP^C to infectious conformers could be accomplished only in the presence of polyanions such as RNA or in a case of recombinant PrP with RNA and synthetic lipids^{19,54}. As a starting point for our sCJD prions (MM1 and MM2)-seeded conversion reactions, we used QuIC in the presence of polyA, Monosialoganglioside GM1 from bovine brain (GM1), or synthetic 2-Oleoyl-1-palmitoyl-sn-glycero-3-phospho-rac-(1-glycerol) (POPG). While the replication and conformational fidelity of MM1 sCJD prions was facilitated by GM1, MM2 sCJD was facilitated by POPG. Considering structural and charge heterogeneity of gangliosides, and their localization together with PrP^C in cholesterol rich domains (caveoli), their distinct characteristics and levels in different cells may explain preferential cellular targeting of different human prions and thus distinct neuropathological profiles. These results support a critical role of cofactors in the strain-specific formation and propagation of human prions, and suggest that different cofactors guide human PrP misfolding in distinct pathways, resulting in different prions. However, whether additional cofactors can also facilitate strain-specific replication of human prions is at present unknown and these initial observations have to be extended with screening of additional cofactors. The obvious potential candidates are phosphatidylglycerol or phosphatidylethanolamine alone, as these cofactors have been shown to facilitate PMCA conversion of bacterially expressed mouse PrP to highly infectious prions^{26,54,55}. Additional human prion strain-specific cofactors can be potentially identified by analysis of nonproteinaceous molecules associated with purified human prions employing a strategy similar to that used previously for identification of rodent prion cofactors^{56–58}. These investigations could open new therapeutic strategies for human prion disease by designing synthetic analogs of auxiliary factors with inhibitory or blocking effect on human prion replication.

Methods

Ethics statement. All procedures were performed under protocols approved by the Institutional Review Board at Case Western Reserve University. In all cases, written informed consent for research was obtained from the patient or legal guardian and the material used had appropriate ethical approval for use in this

project. All patient data and samples were coded and handled according to NIH guidelines to protect patient identities. All animal studies were conducted under the protocols approved by Case Western Reserve University Institutional Animal Care and Use Committee (IACUC).

Patients and clinical evaluations. Prion disease cases were reviewed pertaining to updated diagnostic criteria for sCJD⁵⁹. Brain MRIs were considered positive for CJD if the reading by experienced radiologist fulfilled the criteria defined previously²⁷.

The criteria for inclusion were availability of a clinical diagnosis of CJD according to WHO criteria^{59–62} with dated initial symptoms to ascertain the disease duration; methionine or valine at codon 129 of the human prion protein (PrP) gene (*PRNP*); unequivocal classification of Type 1, Type 2, or Type 1–2 rPrP^{Sc} sCJD according to Western blot (WB) pattern; and unequivocal classification of pathology as definite Type 1, Type 2, or mixed Type 1–2^{63,64}. The criteria for diagnosis of rapidly progressive Alzheimer disease (AD)⁶³ were as follows: probable clinical diagnosis of AD^{63,65}; absent autosomal dominant pattern of dementia; unequivocal classification as AD after detailed neuropathology and immunohistochemistry of tau proteins and amyloid beta using the current National Institute of Aging—Alzheimer's Association guidelines^{63,66}.

CJD Classification, brain samples, and *PRNP* gene sequencing. DNA was extracted from frozen brain tissues in all cases, and genotypic analysis of the *PRNP* coding region was performed as described^{39,67,68}. The CJD cases were classified on the basis of diagnostic pathology, immunohistochemistry, and WB examination of 2 or 3 brain regions (including frontal, occipital and cerebellum cortices) with mAb 3F4^{3,12,29,52}.

For molecular analyses, we used 200–350 mg cuts of frontal (superior and more posterior middle gyri) brain cortex stored at -80°C after autopsy. The other cerebral hemisphere was fixed in formalin and 16 anatomical areas were used for histopathological and immunohistochemical classification of prion disease according to NPDSPC's standard protocols^{3,23,69}. In a case of equivocal classification of sCJD subtype between pathology and Western blots, we based the classification on the molecular characteristics of PrP^{Sc} on Western blots developed with a panel of Type 1 and Type 2-specific antibodies as described previously^{3,70,71}.

Bioassays in transgenic mice expressing human PrP^C (129M). The human PrP^{N181Q/N197Q} ORF, which contains 2 point mutations that change Asn to Gln in amino acid positions 181 and 197, thereby eliminating the two N-linked glycosylation sites on human PrP, was generated by PCR mutagenesis from the human PrP-129M transgene construct used for the generation of the Tg40 mice and described previously⁴⁰. The homozygous TgNN6h line expressing the human PrP^{N181Q/N197Q} ORF at about 60% of the PrP level found in wild type FVB mice was described previously¹². To assay for prion infectivity in the TgNN6h mice, 30 μl of the sample (brain homogenates or recombinant human PrP preparations before or after QuIC) in PBS was injected into the mouse brain with a 26 gauge needle inserted to a depth of about 4 mm at the left parietal region of the cranium and the symptoms monitored as described previously⁴⁰. To prevent cross contamination, the intracerebral inoculations of synthetic prions were performed under sterile conditions in days when no other inoculations were carried out. The animals were housed in microisolator cages and stringent aseptic and biosafety techniques were followed for animal handling and husbandry as we described previously⁴⁰. Within three days after the appearance of symptoms or at death, the animal was euthanized and the brain was removed; one-half was frozen for biochemical studies, and the other half was stored in formalin for histology and immunohistochemistry analysis as described below.

The sCJD brain homogenates. We selected brain samples from a group of sCJD patients, all of whom were methionine or valine homozygous at codon 129 of the human prion protein (PrP) gene (*PRNP*), and who were classified according to pathology and WB pattern as pure Type 1 or Type 2 sCJD at the National Prion Disease Pathology Surveillance Center (NPDSPC) in Cleveland, OH. DNA was extracted from frozen brain tissues in all cases, and genotypic analysis of the *PRNP* coding region was performed as described^{67,68}. All patient data and samples were handled with IRB approval according to NIH guidelines to protect patients' identities and the patients or their legal representatives signed written consent.

Slices of human brain tissues weighing between 200 and 350 mg from the frontal cortex were first homogenized to a final 15% (w/v) in calcium- and magnesium-free PBS, pH 7.4, by using Mini-Beadbeater 16 Cell Disrupter (Biospec, Bartlesville, OK). The homogenates were then diluted to a final 10% (w/v) in PBS / 1% Triton X-100 / 5 mM EDTA / 1 \times Complete PI cocktail (Roche Applied Science, Indianapolis, IN), pH 7.4. They were clarified by a centrifugation at 500 \times g for 5 min, and the collected supernatant was aliquoted and stored at -80°C for QuIC.

QuIC. The QuIC was performed as described⁷² with following modifications. The recombinant human PrP(23–231) with codon 129 M or 129 V used as a substrate in QuIC were expressed, purified, and refolded to α -helical conformation as described previously⁷³. The initial concentration of recombinant human PrP (23–231) was calculated from absorbance at 280 nm and molar extinction

coefficient $56,650 \text{ M}^{-1} \text{ cm}^{-1}$. The stock of rechuPrP(23–231) in 10 mM Sodium Acetate buffer, pH 4.0, was pretreated with 12 mM HCl at 1:5.0 (rechuHuPrP: HCl, v/v) ratio for 7.5 min and immediately diluted to final 0.1 mg/ml into the basic reaction buffer composed of 20 mM NaH_2PO_4 , 130 mM NaCl, pH 6.9. The rechuPrP concentration, QuIC time, and composition of alternative buffers containing 0.1% (v/v) Triton X-100, 1:5000 (v/v) N2 Supplement (Invitrogen, Carlsbad, CA), 0.1% (w/v) SDS, polyadenylic acid (Poly A, Sigma, St. Louis, MO), Monosialoganglioside GM_1 from bovine brain (GM_1 , Avanti Polar Lipids, Alabaster, AL), or synthetic 2-Oleoyl-1-palmitoyl-sn-glycerol-3-phospho-rac-(1-glycerol) (POPG, Sigma, St. Louis, MO) are described in the Supplementary Tables 1, 2, 3, and 4. The QuIC was performed with final volume 100 μl per well in sterile V-bottom, low-binding polypropylene 96-well plate (VWR, Arlington Heights, IL) equipped with a 3 mm diameter PTFE bead (Fisher Scientific, Pittsburg, PA) in each well. The aliquots of sCJD brain homogenates used as seeds were sonicated $3 \times 5 \text{ s}$ at 60% power setting using Misonix Sonicator S-4000 (Qsonica, Newtown, CT), diluted immediately into the complete QuIC reaction buffer to obtain final 10^{-4} dilution of sCJD brain prions, and the plates were sealed with sterile AxyMat[®] Silicone Sealing Mat (VWR, Arlington Heights, IL). The QuIC was performed at 37, 45, or 55 °C for 5 to 96 h in Eppendorf Thermomixer (Eppendorf, Hauppauge, NY) set for 1 min shaking at 1400 rpm followed by 1 min incubation. The control unseeded samples of spontaneously converted prion protein amyloid were prepared according previously published protocol³⁵.

PK treatment. To each well containing 100 μl of QuIC reaction buffer was added 50 μl of PBS, pH 6.9, containing 3% (w/v) Sarcosyl and Proteinase K (PK, Amresco, Solon, OH) to obtain the final Sarcosyl concentration 1% (w/v) and PrP/enzyme ratio 10:1 (w/w) or 100:1 (w/w). The plates was incubated for 1 h at 37 °C at 1200 rpm on the Eppendorf Thermomixer with 1-min. interval. Alternatively, QuIC reaction performed in PBS, pH 6.9 containing 0.5 M NaCl and no detergents was followed with PK treatment without detergents. The PK was blocked in each well with protease inhibitors (0.5 mM PMSF final, and 5 $\mu\text{g}/\text{ml}$ of aprotinin and leupeptin).

SDS PAGE and western blots. The samples were mixed 1:1 with WB (Laemmli Buffer (Bio-Rad, Hercules, CA) containing 5% (v/v) beta-mercaptoethanol (BME), 2% (v/v) SDS, and 115 mM Tris-HCl, pH 6.8 and heated at 100 °C for 5 min. Either 150 ng (silver staining) or 2 ng (Western blots) per lane were loaded on 1 mm 18% Polyacrylamide Tris-HCl, SDS-PAGE gels (Bio-Rad).

SDS-PAGE gels were transblotted to Immobilon-P Transfer Membranes (Millipore, Bedford, MA) in Bio-Rad Western Blot apparatus. The filters were blocked with 5% (w/v) Nonfat milk in TBS containing 0.1% of Tween 20 (v/v) (Sigma, St. Louis, MO), and incubated with one of the following antibodies: mAb 3F4⁷⁴ (epitope residue 107–112); mAb 12B2 (epitope residues 89–93, kindly provided by Jan Langeveld⁷⁵), and mAb 1E4 (epitope residues 97–108, Cell Sciences, Canton, MA). After incubation with secondary anti-mouse IgG peroxidase-labeled sheep Ab (Amersham, Piscataway, NJ), the membranes were developed with the ECL Plus detection system (Amersham) and exposed to Kodak BioMax MR Films (Fisher Scientific) or Kodak BioMax XAR Films (Fisher Scientific).

Histology and immunohistochemistry lesion profiles. We used hematoxylin and eosin or antibody 3F4 on four different coronal sections for the histopathology and immunohistochemical detection of PrP^{Sc} in rodent brains as reported previously^{39,76,77}. Semiquantitative evaluation of spongiosis and gliosis was performed by comparing hematoxylin and eosin-stained sections using a modified procedure of Fraser and Dickinson⁷⁸. Nine areas of gray matter were examined, and a score was given for the severity of spongiform degeneration using the scale based on a number and confluency of vacuoles in the field at 400-fold magnification: 0, no vacuoles; 1, one to three vacuoles widely and unevenly distributed; 2, on average ten vacuoles evenly scattered; 3, on average thirty vacuoles evenly scattered; 4, on average 90 vacuoles with some confluences; 5, dense vacuolation with prominent confluence.

Thioflavin S staining. After deparaffinization, formalin-fixed sections were stained in Thioflavin S for 7 min, washed three times in 80% alcohol, dehydrated in ethanol, cleared in xylene, and cover slipped with Vectashield mounting medium for fluorescence. Sections were kept in the dark at 4 °C for 30 min before being viewed under the fluorescence microscope (Olympus IX71).

Conformation-dependent immunoassay (CDI). The CDI for human PrP was performed as described previously^{39,79}, with following modifications: white Lumitrac 600 High Binding Plates (E&K Scientific, Santa Clara, CA) were coated with mAb 8H4 (epitope 175–185)⁸⁰ and aliquots of each sample containing 0.007% (v/v) of Patent Blue V (Sigma) were diluted into plate wells filled with 200 μl of Assay Buffer (Perkin Elmer, Waltham, MA); he captured PrP was detected by a europium-conjugated⁸¹ anti-PrP mAb 3F4 (epitope 108–112)⁷⁴ and the time-resolved fluorescence (TRF) signals were measured by the multi-mode microplate reader PHERAstar Plus (BMG LabTech, Durham, NC).

Conformational stability assay (CSA) of prions. The sequential denaturation of human PrP^{Sc} was performed as described previously⁸¹, with several modifications. Frozen aliquots of PrP^{Sc} were thawed, sonicated $3 \times 5 \text{ s}$ at 60% power with Sonicator 4000 (Qsonica, Newtown, CT); and the concentration was adjusted to constant $\sim 50 \text{ ng}/\text{ml}$ of PrP^{Sc} or rhuPrion. The 15 μl aliquots in 15 tubes were treated with increasing concentrations of 8 M GdnHCl containing 0.007% (v/v) Patent Blue V (Sigma, St. Louis, MO) in 0.25 M or 0.5 M increments. After 30 min incubation at room temperature, individual tubes were rapidly diluted with Assay Buffer (Perkin Elmer, Waltham, MA) containing diminishing concentrations of 8 M GdnHCl, so that the final concentration in all samples was 0.411 M. Each individual aliquot was immediately loaded in triplicates to dry white Lumitrac 600, High Binding Plates (E&K Scientific, Santa Clara, CA), coated with mAb 8H4, and developed in accordance with CDI protocol using europium-labeled mAb 3F4 for detection^{39,81–83}. The raw TRF signal was converted into the apparent fractional change of unfolding (Fapp) as follows: $F_{\text{app}} = (\text{TRF}_{\text{OBS}} - \text{TRF}_{\text{N}}) / (\text{TRF}_{\text{U}} - \text{TRF}_{\text{N}})$ where TRF_{OBS} is the observed TRF value, and TRF_{N} and TRF_{U} are the TRF values for native and unfolded forms, respectively, at the given Gdn HCl concentration⁵. To determine the concentration of Gdn HCl where 50% of PrP^{Sc} is unfolded ($[\text{Gdn HCl}]_{1/2}$), the data were fitted by least square method with a sigmoidal transition model as described previously⁵².

Second-generation RT-QuIC. The second-generation RT-QuIC assays were performed as previously described, with minor modifications¹⁸. The RT-QuIC reaction mix was prepared as follows: 10 mM phosphate buffer (pH 7.4), 300 mM NaCl, 0.1 mg/ml SHarPrP(23–231), 10 μM thioflavin T (ThT), 1 mM ethylenediaminetetraacetic acid tetrasodium salt (EDTA) and 0.002% sodium dodecyl sulfate (SDS). The 85 μl of reaction mix was loaded into each plate well and seeded with 15 μl of brain homogenates for a final reaction volume of 100 μl . The incubation and real time fluorescence monitoring was performed using the FLUOstar Omega plate reader (BMG LABTECH GmbH, Ortenberg, Germany) set to the following parameters: 55 °C incubation, 60 h reaction time, 60 s shake/60 s rest cycles with ThT fluorescence measurements taken every 45 min.

HXMS experiments. The pellets containing aggregates of rechuPrP after PK treatment were washed three times in H_2O . For deuterium labeling, pellets ($\sim 20 \mu\text{l}$) were resuspended in 400 μl of the buffer (10 mM phosphate, pH 7.0) prepared in D_2O . After incubation at room temperature for different time periods, samples were centrifuged at $21,000 \times g$ for 5 min and dissociated by incubating for 5 min on ice in a quenching buffer (0.1 M phosphate, pH 2.4) containing 7 M guanidine hydrochloride and 0.1 M TCEP [Tris(2-carboxyethyl)phosphine hydrochloride]. The samples were then diluted 10 times with an ice cold 0.05% TFA (Trifluoroacetic acid) and digested for 5 min with agarose-immobilized pepsin (Thermo Scientific). The peptic fragments were separated and analyzed by mass spectrometry as described previously^{34,35}.

His-HXMS experiments. For these measurements, the pellets containing aggregates of rhuPrP after PK treatment ($\sim 3.6 \mu\text{g}$) were suspended in D_2O buffer (10 mM sodium phosphate, pH 9.0) and incubated for 5 days at 37 °C. Following incubation, samples were collected by centrifugation. To obtain peptide fragments containing single His residues, the aggregates were dissociated with 7 M Gdn and digested first with agarose-immobilized pepsin and then silica-immobilized trypsin as described previously¹⁶. The peptic fragments were separated on an UPLC column and analyzed by mass spectrometry on an LTQ Orbitrap mass spectrometer. Mass spectrometric data were analyzed and half-life ($t_{1/2}$, days) of His exchange reaction was determined as described previously¹⁶.

Statistical analysis. We compared the parameters for the whole group and different phenotypic subgroups with ANOVA or Fisher exact test. Cumulative survival curves were constructed by the Kaplan–Meier method and compared using the Mantel-Cox and Breslow methods. For each type of PrP^{Sc} and PRNP codon 129 polymorphism, we report descriptive statistics and each variable was compared with ANOVA.

Data availability. All data supporting the findings in this study are available within the article and Supporting files, or are available from the corresponding author upon reasonable request.

Received: 20 February 2018 Accepted: 2 May 2018

Published online: 04 June 2018

References

- Gajdusek, D. C., Gibbs, C. J. Jr. & Alpers, M. Experimental transmission of a kuru-like syndrome to chimpanzees. *Nature* **209**, 794–796 (1966).
- Prusiner, S. B., Scott, M. R., DeArmond, S. J. & Carlson, G. Transmission and replication of prions. in *Prion Biology and Diseases* (Prusiner, S. B. ed.) 187–242 (Cold Spring Harbor Laboratory Press, Cold Spring Harbor, 2004).

3. Puoti, G. et al. Sporadic human prion diseases: molecular insights and diagnosis. *Lancet Neurol.* **11**, 618–628 (2012).
4. Prusiner, S. B. Novel proteinaceous infectious particles cause scrapie. *Science* **216**, 136–144 (1982).
5. Safar, J., Roller, P. P., Gajdusek, D. C. & Gibbs, C. J. Jr. Conformational transitions, dissociation, and unfolding of scrapie amyloid (prion) protein. *J. Biol. Chem.* **268**, 20276–20284 (1993).
6. Prusiner, S. B. Prions. *Proc. Natl Acad. Sci. USA* **95**, 13363–13383 (1998).
7. Prusiner, S. B. ed. *Prion Biology and Diseases*, 1050 (Cold Spring Harbor Laboratory Press, Cold Spring Harbor, 2004).
8. Caughey, B., Baron, G. S., Chesebro, B. & Jeffrey, M. Getting a grip on prions: oligomers, amyloids, and pathological membrane interactions. *Annu. Rev. Biochem.* **78**, 177–204 (2009).
9. Cobb, N. J. & Surewicz, W. K. Prion diseases and their biochemical mechanisms. *Biochemistry* **48**, 2574–2585 (2009).
10. Collinge, J. & Clarke, A. R. A general model of prion strains and their pathogenicity. *Science* **318**, 930–936 (2007).
11. Morales, R., Abid, K. & Soto, C. The prion strain phenomenon: molecular basis and unprecedented features. *Biochim. Biophys. Acta* **1772**, 681–691 (2007).
12. Haldiman, T. et al. Co-existence of distinct prion types enables conformational evolution of human PrPSc by competitive selection. *J. Biol. Chem.* **288**, 29846–29861 (2013).
13. Geschwind, M. D. et al. Quinacrine treatment trial for sporadic Creutzfeldt-Jakob disease. *Neurology* **81**, 2015–2023 (2013).
14. Collinge, J. et al. Safety and efficacy of quinacrine in human prion disease (PRION-1 study): a patient-preference trial. *Lancet Neurol.* **8**, 334–344 (2009).
15. Haik, S. et al. Doxycycline in Creutzfeldt-Jakob disease: a phase 2, randomised, double-blind, placebo-controlled trial. *Lancet Neurol.* **13**, 150–158 (2014).
16. Safar, J. G. et al. Structural determinants of phenotypic diversity and replication rate of human prions. *PLoS Pathog.* **11**, e1004832 (2015).
17. Orru, C. D. et al. Prion seeding activity and infectivity in skin samples from patients with sporadic Creutzfeldt-Jakob disease. *Sci. Transl. Med.* **9**, eaam7785 (2017).
18. Foutz, A. et al. Diagnostic and prognostic value of human prion detection in cerebrospinal fluid. *Ann. Neurol.* **81**, 79–92 (2017).
19. Deleault, N. R., Harris, B. T., Rees, J. R. & Supattapone, S. Formation of native prions from minimal components in vitro. *Proc. Natl Acad. Sci. USA* **104**, 9741–9746 (2007).
20. Makarava, N. et al. Recombinant prion protein induces a new transmissible prion disease in wild-type animals. *Acta Neuropathol.* **119**, 177–187 (2010).
21. Zhang, Z. et al. De novo generation of infectious prions with bacterially expressed recombinant prion protein. *Faseb J.* **27**, 4768–4775 (2013).
22. Legname, G. et al. Strain-specified characteristics of mouse synthetic prions. *Proc. Natl Acad. Sci. USA* **102**, 2168–2173 (2005).
23. Kim, J. I. et al. Mammalian prions generated from bacterially expressed prion protein in the absence of any mammalian cofactors. *J. Biol. Chem.* **285**, 14083–14087 (2010).
24. Theint, T., Nadaud, P. S., Surewicz, K., Surewicz, W. K. & Jaronic, C. P. 13C and 15N chemical shift assignments of mammalian Y145Stop prion protein amyloid fibrils. *Biomol. NMR Assign.* **11**, 75–80 (2017).
25. Choi, J. K. et al. Amyloid fibrils from the N-terminal prion protein fragment are infectious. *Proc. Natl Acad. Sci. USA* **113**, 13851–13856 (2016).
26. Noble, G. P. et al. A structural and functional comparison between infectious and non-infectious autocatalytic recombinant PrP conformers. *PLoS Pathog.* **11**, e1005017 (2015).
27. Klingeborn, M., Race, B., Meade-White, K. D. & Chesebro, B. Lower specific infectivity of protease-resistant prion protein generated in cell-free reactions. *Proc. Natl Acad. Sci. USA* **108**, E1244–E1253 (2011).
28. Haldiman, T. et al. Co-existence of distinct prion types enables conformational evolution of human PrPSc by competitive selection*. *J. Biol. Chem.* **288**, 29846–29861 (2013).
29. Kim, C. et al. Small protease sensitive oligomers of PrP(Sc) in distinct human prions determine conversion rate of PrP(C). *PLoS Pathog.* **8**, e1002835 (2013).
30. Korth, C. et al. Abbreviated incubation times for human prions in mice expressing a chimeric mouse–human prion protein transgene. *Proc. Natl Acad. Sci. USA* **100**, 4784–4789 (2003).
31. Bishop, M. T., Will, R. G. & Manson, J. C. Defining sporadic Creutzfeldt-Jakob disease strains and their transmission properties. *Proc. Natl Acad. Sci. USA* **107**, 12005–12010 (2010).
32. Giles, K. et al. Human prion strain selection in transgenic mice. *Ann. Neurol.* **68**, 151–161 (2010).
33. Cobb, N. J., Apostol, M. I., Chen, S., Smirnovas, V. & Surewicz, W. K. Conformational stability of mammalian prion protein amyloid fibrils is dictated by a packing polymorphism within the core region. *J. Biol. Chem.* **289**, 2643–2650 (2014).
34. Smirnovas, V. et al. Structural organization of brain-derived mammalian prions examined by hydrogen-deuterium exchange. *Nat. Struct. Mol. Biol.* **18**, 504–506 (2011).
35. Smirnovas, V. et al. Distinct structures of scrapie prion protein (PrPSc)-seeded versus spontaneous recombinant prion protein fibrils revealed by hydrogen/deuterium exchange. *J. Biol. Chem.* **284**, 24233–24241 (2009).
36. Aguilar-Calvo, P. et al. Post-translational modifications in PrP expand the conformational diversity of prions in vivo. *Sci. Rep.* **7**, 43295 (2017).
37. Mullangi, V., Zhou, X., Ball, D. W., Anderson, D. J. & Miyagi, M. Quantitative measurement of the solvent accessibility of histidine imidazole groups in proteins. *Biochemistry* **51**, 7202–7208 (2012).
38. Lu, X., Wintrode, P. L. & Surewicz, W. K. Beta-sheet core of human prion protein amyloid fibrils as determined by hydrogen/deuterium exchange. *Proc. Natl Acad. Sci. USA* **104**, 1510–1515 (2007).
39. Safar, J. G. et al. Diagnosis of human prion disease. *Proc. Natl Acad. Sci. USA* **102**, 3501–3506 (2005).
40. Kong, Q. et al. Chronic wasting disease of elk: transmissibility to humans examined by transgenic mouse models. *J. Neurosci.* **25**, 7944–7999 (2005).
41. Hornemann, S., Schorn, C. & Wuthrich, K. NMR structure of the bovine prion protein isolated from healthy calf brains. *EMBO Rep.* **5**, 1159–1164 (2004).
42. Safar, J., Ceroni, M., Gajdusek, D. C. & Gibbs, C. J. Jr. Differences in the membrane interaction of scrapie amyloid precursor proteins in normal and scrapie- or Creutzfeldt-Jakob disease-infected brains. *J. Infect. Dis.* **163**, 488–494 (1991).
43. Oelschlegel, A. M. & Weissmann, C. Acquisition of drug resistance and dependence by prions. *PLoS Pathog.* **9**, e1003158 (2013).
44. Groveman, B. R. et al. Role of the central lysine cluster and scrapie templating in the transmissibility of synthetic prion protein aggregates. *PLoS Pathog.* **13**, e1006623 (2017).
45. Wiseman, F. K. et al. The glycosylation status of PrPC is a key factor in determining transmissible spongiform encephalopathy transmission between species. *J. Virol.* **89**, 4738–4747 (2015).
46. Katorcha, E., Makarava, N., Savtchenko, R. & Baskakov, I. V. Sialylation of the prion protein glycans controls prion replication rate and glycoform ratio. *Sci. Rep.* **5**, 16912 (2015).
47. Morales, R. et al. Strain-dependent profile of misfolded prion protein aggregates. *Sci. Rep.* **6**, 20526 (2016).
48. Parchi, P. et al. Typing prion isoforms. *Nature* **386**, 232–233 (1997).
49. Telling, G. C. et al. Evidence for the conformation of the pathologic isoform of the prion protein enciphering and propagating prion diversity. *Science* **274**, 2079–2082 (1996).
50. Collinge, J., Sidle, K. C. L., Meads, J., Ironside, J. & Hill, A. F. Molecular analysis of prion strain variation and the aetiology of “new variant” CJD. *Nature* **383**, 685–690 (1996).
51. Cracco, L. et al. Novel strain properties distinguishing sporadic prion diseases sharing prion protein genotype and prion type. *Sci. Rep.* **7**, 38280 (2017).
52. Kim, C. et al. Protease-sensitive conformers in broad spectrum of distinct PrP structures in sporadic Creutzfeldt-Jakob disease are indicator of progression rate. *PLoS Pathog.* **7**, e1002242 (2011).
53. Klein, T. R., Kirsch, D., Kaufmann, R. & Riesner, D. Prion rods contain small amounts of two sphingolipids as revealed by thin-layer chromatography and mass spectrometry. *J. Biol. Chem.* **379**, 655–666 (1998).
54. Wang, F., Wang, X., Yuan, C. G. & Ma, J. Generating a prion with bacterially expressed recombinant prion protein. *Science* **327**, 1132–1135 (2010).
55. Noble, G. P., Walsh, D. J., Miller, M. B., Jackson, W. S. & Supattapone, S. Requirements for mutant and wild-type prion protein misfolding in vitro. *Biochemistry* **54**, 1180–1187 (2015).
56. Supattapone, S. Synthesis of high titer infectious prions with cofactor molecules. *J. Biol. Chem.* **289**, 19850–19854 (2014).
57. Deleault, N. R. et al. Cofactor molecules maintain infectious conformation and restrict strain properties in purified prions. *Proc. Natl Acad. Sci. USA* **109**, E1938–46 (2012).
58. Deleault, N. R. et al. Isolation of phosphatidylethanolamine as a solitary cofactor for prion formation in the absence of nucleic acids. *Proc. Natl Acad. Sci. USA* **109**, 8546–8551 (2012).
59. Zerr, I. et al. Updated clinical diagnostic criteria for sporadic Creutzfeldt-Jakob disease. *Brain* **132**, 2659–2668 (2009).
60. World Health Organization. WHO infection control guidelines for transmissible spongiform encephalopathies. (World Health Organization Emerging and other Communicable Diseases, S.a.C. ed.) 38 (Geneva, 1999).
61. Collins, S. J. et al. Determinants of diagnostic investigation sensitivities across the clinical spectrum of sporadic Creutzfeldt-Jakob disease. *Brain* **129**, 2278–2287 (2006).
62. Geschwind, M. D., Shu, H., Haman, A., Sejvar, J. J. & Miller, B. L. Rapidly progressive dementia. *Ann. Neurol.* **64**, 97–108 (2008).
63. Cohen, M. L. et al. Rapidly progressive Alzheimer’s disease features distinct structures of amyloid-beta. *Brain* **138**, 1009–1022 (2015).

64. Chitravas, N. et al. Treatable neurological disorders misdiagnosed as Creutzfeldt-Jakob disease. *Ann. Neurol.* **70**, 437–444 (2011).
65. McKhann, G. M. et al. The diagnosis of dementia due to Alzheimer's disease: recommendations from the National Institute on Aging-Alzheimer's Association workgroups on diagnostic guidelines for Alzheimer's disease. *Alzheimers Dement.* **7**, 263–269 (2011).
66. Josephs, K. A. & Nelson, P. T. Unlocking the mysteries of TDP-43. *Neurology* **84**, 870–871 (2015).
67. Parchi, P. et al. Genetic influence on the structural variations of the abnormal prion protein. *Proc. Natl Acad. Sci. USA* **97**, 10168–10172 (2000).
68. Parchi, P. et al. Molecular basis of phenotypic variability in sporadic Creutzfeldt-Jakob disease. *Ann. Neurol.* **39**, 767–778 (1996).
69. Gambetti, P., Kong, Q., Zou, W., Parchi, P. & Chen, S. G. Sporadic and familial CJD: classification and characterisation. *Br. Med. Bull.* **66**, 213–239 (2003).
70. Parchi, P. et al. Consensus classification of human prion disease histotypes allows reliable identification of molecular subtypes: an inter-rater study among surveillance centres in Europe and USA. *Acta Neuropathol.* **124**, 517–529 (2012).
71. Cali, I. et al. Co-existence of scrapie prion protein types 1 and 2 in sporadic Creutzfeldt-Jakob disease: its effect on the phenotype and prion-type characteristics. *Brain* **132**, 2643–2658 (2009).
72. Atarashi, R. et al. Simplified ultrasensitive prion detection by recombinant PrP conversion with shaking. *Nat. Methods* **5**, 211–212 (2008).
73. Swietnicki, W., Morillas, M., Chen, S. G., Gambetti, P. & Surewicz, W. K. Aggregation and fibrillization of the recombinant human prion protein huPrP90-231. *Biochemistry* **39**, 424–431 (2000).
74. Kacsak, R. J. et al. Mouse polyclonal and monoclonal antibody to scrapie-associated fibril proteins. *J. Virol.* **61**, 3688–3693 (1987).
75. Thuring, C. M. et al. Discrimination between scrapie and bovine spongiform encephalopathy in sheep by molecular size, immunoreactivity, and glycoprofile of prion protein. *J. Clin. Microbiol.* **42**, 972–980 (2004).
76. Safar, J. G. et al. Transmission and detection of prions in feces. *J. Infect. Dis.* **198**, 81–89 (2008).
77. Tamgüney, G. et al. Transmission of Elk and Deer prions to transgenic mice†. *J. Virol.* **80**, 9104–9114 (2006).
78. Fraser, H. & Dickinson, A. G. The sequential development of the brain lesions of scrapie in three strains of mice. *J. Comp. Pathol.* **78**, 301–311 (1968).
79. Choi, E. M. et al. Prion proteins in subpopulations of white blood cells from patients with sporadic Creutzfeldt-Jakob disease. *Lab. Invest.* **89**, 624–635 (2009).
80. Zanusso, G. et al. Prion protein expression in different species: analysis with a panel of new mAbs. *Proc. Natl Acad. Sci. USA* **95**, 8812–8816 (1998).
81. Safar, J. et al. Eight prion strains have PrP^{Sc} molecules with different conformations. *Nat. Med.* **4**, 1157–1165 (1998).
82. Safar, J. G. et al. Human prions and plasma lipoproteins. *Proc. Natl Acad. Sci. USA* **103**, 11312–11317 (2006).
83. Safar, J. G. et al. Measuring prions causing bovine spongiform encephalopathy or chronic wasting disease by immunoassays and transgenic mice. *Nat. Biotechnol.* **20**, 1147–1150 (2002).

Acknowledgements

The authors are grateful to the patients' families, the CJD Foundation, referring clinicians, and all the members of the National Prion Disease Pathology Surveillance Center for invaluable technical help. We thank Dr. Mentor Mulaj for help with obtaining circular dichroism data shown in Supplementary Figure S2, Dr. Man-Sun Sy for making available hybridoma clone 8H4, and Dr. Earl Poptic for scaled up antibody production. This work was supported by the Centers for Disease Control and Prevention (grant UR8/CCU515004 to JGS), the National Institutes of Health grants NS074317 (to JGS), NS 060729 (to WKS), AI106705 (to WKS), and the Charles S. Britton Fund (to JGS).

Author contributions

Conceived and designed the experiments: J.G.S., W.K.S. Performed the prion conversion and mass spectrometry experiments: C.K., T.H., X.X., S.C., V.S., K.S. Performed the bioassays: Q.K., N.R.M. Performed the pathology and immunohistochemistry: J.G.S., D. K., M.W. Analyzed the data: J.G.S., W.K.S., X.X., S.C., Q.K. Wrote the paper: J.G.S., W.K.S.

Additional information

Supplementary Information accompanies this paper at <https://doi.org/10.1038/s41467-018-04584-z>.

Competing interests: The authors declare no competing interests.

Reprints and permission information is available online at <http://npg.nature.com/reprintsandpermissions/>

Publisher's note: Springer Nature remains neutral with regard to jurisdictional claims in published maps and institutional affiliations.



Open Access This article is licensed under a Creative Commons Attribution 4.0 International License, which permits use, sharing, adaptation, distribution and reproduction in any medium or format, as long as you give appropriate credit to the original author(s) and the source, provide a link to the Creative Commons license, and indicate if changes were made. The images or other third party material in this article are included in the article's Creative Commons license, unless indicated otherwise in a credit line to the material. If material is not included in the article's Creative Commons license and your intended use is not permitted by statutory regulation or exceeds the permitted use, you will need to obtain permission directly from the copyright holder. To view a copy of this license, visit <http://creativecommons.org/licenses/by/4.0/>.

© The Author(s) 2018